PAPER

Check for updates

Synthesis of novel porphyrin derivatives and their self-assemblies to enhance photocatalytic performance†

Jinghe Pei,[a] Bo Gao, ⁑[ab] Yanhui Li [a] and Qian Duan ⁑[a]

Three new porphyrin derivatives were synthesized from tetra (4-aminophenyl) porphyrin (TAPP), namely tetra[*p*-(4-cyanophenylmethylene imino)]phenyl porphyrin (TCyPPP), tetra[*p*-(*P*-benzylidene)]phenyl porphyrin (TbePPP) and tetra[*p*-(4-pyridylmethylene imino)]phenyl porphyrin (TPyPPP). Based on the principle of self-assembly, three kinds of porphyrin derivatives were self-assembled to prepare three kinds of monomers. The structures were characterized clearly by UV-vis, FT-IR, ^{1}H NMR and SEM. The photocatalytic performance study shows that the self-assemblies of the three porphyrin derivatives have stronger photocatalytic performance than their monomers. Moreover, the self-assemblies and their monomers have good photocatalytic stability.

Introduction

Porphyrin, as a natural aromatic cyclic compound, has unique physical properties and can be used in catalytic energy storage and optoelectronic devices for energy conversion, photodynamic therapy, sensors and photonics.[1–5] Unfortunately, the absorption range of the porphyrin monomer in the visible light region is relatively narrow and it is easily corroded by light.[6] It is shown that the design of the porphyrin molecular structure and the accumulation of porphyrin molecules can effectively affect the ability to separate photogenic carriers.[7]

In recent years, a large amount of wastewater containing organic pollutants has been discharged into the natural water system, causing serious water pollution problems.[8,9] As an economical and environmentally friendly technology, photocatalytic technology is more and more popular. The idea of eliminating organic pollutants by using solar energy makes photocatalytic technology a potential technology to solve the environmental problems faced by human beings.[10] For the self-assembly of porphyrin, more and more applications in photocatalytic degradation have been seen in recent years.[11,12] Porphyrin self-assembly is widely used in sensing, photocollection and photocatalytic degradation due to its excellent

photochemistry, photophysics, electrochemistry and other excellent properties.[13–17]

Self-assembly is based on the interaction forces between porphyrin molecules (such as hydrogen bonds, π–π stacking, hydrophilic or hydrophobic interactions, ligand coordination, *etc.*) to achieve accumulation and arrangement between molecules in order to form porphyrin self-assembled nanoparticles.[18–20] In recent years, the self-assembly of porphyrins has been more and more popular, and self-assembled nanoparticles of porphyrins have been synthesized by many methods.[21–27] Yong Zhong *et al.* prepared porphyrin self-assembled nanostructures with lamellar, octahedral and microsphere morphologies, and investigated the effect of the porphyrin self-assembled morphologies on the photocatalytic performance.[28] Peipei Guo prepared a one-dimensional supramolecular ZnTPyP nanometer assembly using the surfactant-assisted self-assembly method and using GO as the surfactant, which shows superior photocatalytic activity compared with the conventional surfactant preparation method.[29] Duong Duc La *et al.* assembled a TiO$_2$@porphyrin hybrid material by means of collaborative self-assembly, and the material exhibited highly efficient photocatalytic activity under simulated sunlight.[30,31] Dong Wang *et al.* also used tetrapyridine zinc porphyrin as the assembly unit to self-assemble ZnTPyP@NO porphyrin nanoparticles by an acid–base neutralization-micellar limited self-assembly method, which significantly enhanced the antibacterial activity.[32]

Since the discovery of Schiff base chemistry and its important application in catalyst science, it has been widely used in the modification of porphyrin compounds.[33] Based on these results, tetra(4-aminophenyl)porphyrin (TAPP) was combined with *p*-cyanobenzaldehyde benzaldehyde and 4-pyridinyl
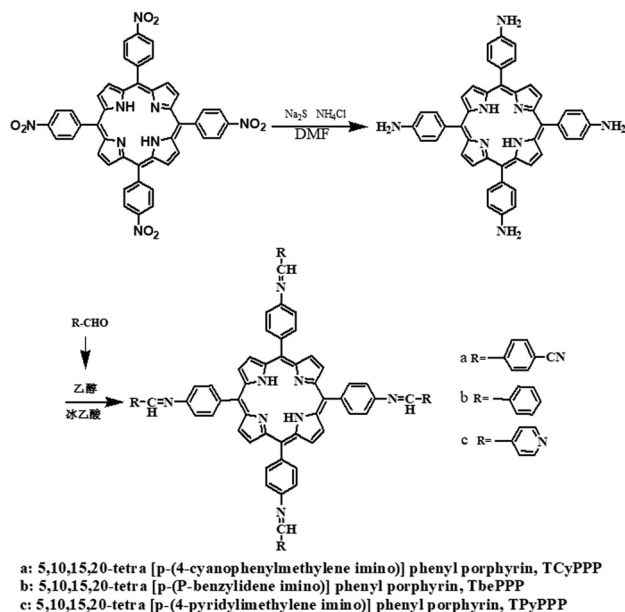
[a] School of Materials Science and Engineering, Changchun University of Science and Technology, 7989 Weixing Road, Changchun 130022, China.
E-mail: gaobo@ciac.ac.cn, duanqian88@hotmail.com; Fax: +86-431-85583015;
Tel: +86-431-85583015

[b] Engineering Research Center of Optoelectronic Functional Materials, Ministry of Education, Changchun 130022, China

† Electronic supplementary information (ESI) available. See DOI: 10.1039/d0nj05297c

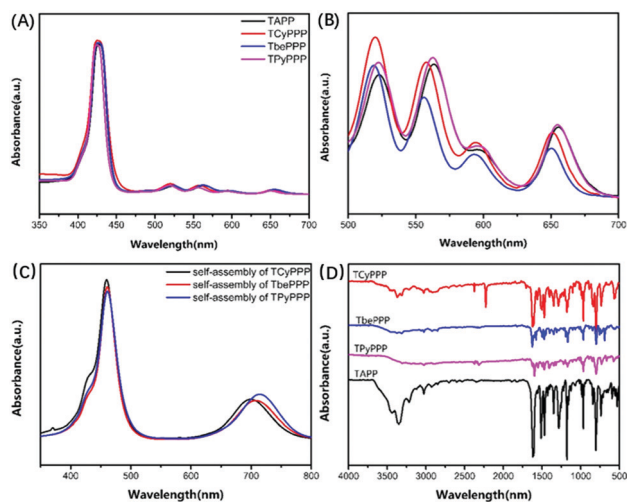**Scheme 1** Synthesis routes of TCyPPP, TbePPP and TPyPPP.

Fig. 1 (A) UV-vis spectra of TAPP, TCyPPP, TbePPP and TPyPPP. (B) UV-vis spectra of TAPP, TCyPPP, TbePPP and TPyPPP in the range of 500–700 nm. (C) Self-assembly of TCyPPP, TbePPP and TPyPPP. (D) The FT-IR spectra of TAPP and TCyPPP, TbePPP and TPyPPP.

formaldehyde in the form of a Schiff base, and three new porphyrin–Schiff base conjugates were synthesized, as shown in Scheme 1. Finally, the three porphyrin derivatives were self-assembled based on the principle of self-assembly, and the monomer and its self-assembly were used in a photocatalytic degradation experiment of rhodamine B in visible light, their photocatalytic performance was evaluated, and the corresponding photocatalytic mechanism was proposed.

Experimental

Materials and characterization

The TNPP used was prepared in the laboratory with pyrrole and p-nitrobenzaldehyde as raw materials, and pyrrole had to be distilled prior to use. All other chemicals were purchased from Sinopharm Chemical Reagent Co. and were used as received. ^{1}H NMR spectra were recorded on a Bruker Avance 500 MHz spectrometer using CDCl$_3$ as a solvent at ambient temperature. FT-IR measurements were performed on KBr pellets on a Shimadzu-8400SIR spectrometer. UV-vis spectra of the samples were recorded over different irradiation time intervals using a Thermo Scientific Evolution 220 spectrophotometer. SEM was performed using a JEM-6701F with an Oxford INCA PentaFET-x3 EDS system. X-Ray diffraction (XRD) patterns were recorded on a RigakuUltima VI diffractometer using Cu-Kα radiation.

Synthesis of 5,10,15,20-tetra(4-aminophenyl)-21h,23h-porphyrin (TAPP). 500 mg TNPP, 2.6 g Na$_2$S and 160 mg NH$_4$Cl were dissolved in 50 mL DMF and reacted at 70 °C for 8 h. After cooling, they were filtered, washed with deionized water, and dried in a vacuum. After purification by column chromatography, the purple powder solid TAPP was obtained (Fig. S1, ESI†).

FT-IR (KBr, cm^{-1}): 3440 ($\nu_{vs\,N-H}$, amino), 3348 (ν_{N-H}, pyrrole), 1350 (ν_{N-H}, amino), 1470 ($\nu_{C=N}$, pyrrole), 1285 (ν_{C-N}, amino)

(Fig. 1A). ^{1}H NMR (500 MHz, CDCl$_3$), δ ppm: 8.90 (s, 8H, C–H, pyrrole), 7.99 (d, 8H, Ar-H), 7.08 (d, 8H, Ar-H), 5.29 (s, 8H, PH-NH$_2$), −2.72 (s, 2H, –NH– pyrrole) (Fig. S2, ESI†).

Synthesis of porphyrin derivatives TCyPPP, TbePPP and TPyPPP. 0.5 g (0.7 mmol) TAPP, 60 mL ethanol and 3.5 mmol aldehyde were stirred and dissolved. A little glacial acetic acid was added as a catalyst. The solution was refluxed at 90 °C for 8 h, and left to rest until the reaction was over. It was then filtered and washed with anhydrous ethanol until the filtrate was colorless and vacuum dried.

Tetra[p-(4-cyanophenylmethylene imino)]phenyl porphyrin (TCyPPP). According to the above method, 0.5 g (0.7 mmol) TAPP and 0.46 g (3.5 mmol) p-cyanobenzaldehyde were taken to prepare compound TCyPPP.

FT-IR (KBr, cm^{-1}): 3364 (ν_{N-H}, pyrrole), 2229 (ν_{-CN}, phenyl), 1613 ($\nu_{C=N}$, –N=CH–), 1467 ($\nu_{C=C}$, phenyl), 1179 ($\nu_{C=N}$, pyrrole) are the skeletal vibrations of pyrrole (Fig. 1D). ^{1}H NMR (500 MHz, CDCl$_3$), δ ppm: 10.06 (s, 8H, C–H, pyrrole), 8.94 (s, 4H, –N=CH–), 8.27–8.25 (d, J = 8.0 Hz, 8H, phenyl), 7.94–7.96 (d, J = 8.0 Hz, 8H, phenyl), 7.62–7.64 (d, J = 8.0 Hz, 8H, phenyl), 7.08–7.10 (d, J = 8.0 Hz, 8H, phenyl), −2.74 (s, 2H, –NH– pyrrole) (Fig. S3, ESI†).

Tetra[p-(P-benzylidene imino)]phenyl porphyrin (TbePPP). According to the above methods, 0.5 g (0.7 mmol) TAPP and 360 μL (3.5 mmol) benzaldehyde were used to prepare compound TbePPP.

FT-IR (KBr, cm^{-1}): 3313 (ν_{N-H}, pyrrole), 1623 ($\nu_{C=N}$, Schiff base), 1471 ($\nu_{C=C}$, phenyl), 1175 ($\nu_{C=N}$, pyrrole) (Fig. 1D). ^{1}H NMR (500 MHz, CDCl$_3$), δ ppm: 10.03 (s, 8H, C–H, pyrrole), 8.95 (s, 4H, –N=CH–), 8.81–8.79 (d, J = 8.0 Hz, 8H, phenyl), 8.24–8.22 (d, J = 8.0 Hz, 8H, phenyl), 8.07–8.05 (d, J = 8.0 Hz, 8H, phenyl), 7.56–7.54 (d, J = 8.0 Hz, 8H, phenyl), 7.03 (s, 8H, phenyl), −2.70 (s, 2H, –NH– pyrrole) (Fig. S4, ESI†).

Tetra[p-(4-pyridylimethylene imino)]phenyl porphyrin (TPyPPP). According to the above method, 0.5 g (0.7 mmol) TAPP and 336 μL 4-pyridyl formaldehyde (3.5 mmol) were used to prepare compound TPyPPP.

FT-IR (KBr, cm^{-1}): 3308 (ν_{N-H}, pyrrole), 3029 (ν_{C-H}, pyridyl), 1603 ($\nu_{C=N}$, –N=CH–), 1471 ($\nu_{C=C}$, phenyl), 1171 ($\nu_{C=N}$, pyrrole) (Fig. 1D). ^{1}H NMR (500 MHz, CDCl$_3$), δ ppm: 10.05 (s, 8H, C–H, pyrrole), 8.81 (s, 4H, –N=CH–), 8.27–8.25 (d, J = 8.0 Hz, 8H, phenyl), 8.76–7.74 (d, J = 8.0 Hz, 8H, phenyl), 7.61–7.59 (d, J = 8.0 Hz, 8H, phenyl), 7.05–7.03 (d, J = 8.0 Hz, 8H, phenyl), −2.71 (s, 2H, –NH– pyrrole) (Fig. S5, ESI†).

Self-assembly of TCyPPP, TbePPP and TPyPPP monomers. Three monomers of TCyPPP, TbePPP and TPyPPP were self-assembled by a simple solution method. Three monomers of 1 mg were respectively put into three small beakers and dissolved with tetrahydrofuran. The concentrated sulfuric acid-coated slides were then placed in a small beaker to allow the solution to submerge the slides. The beakers were placed in a fume hood and tetrahydrofuran was allowed to evaporate slowly. In the process of volatilization, the three monomers are self-assembled on the glass sheet, and the self-assembly is attached to the slide during the process of self-assembly. After tetrahydrofuran was completely evaporated, the self-assembly attached to the slide was carefully scraped and collected.

Photocatalytic degradation measurement

A rhodamine B solution was prepared at a concentration of 1 × 10^{-5} mol L^{-1}, 40 mL was taken out and put into a xenon lamp reactor, about 1 mL of hydrogen peroxide was added, and 5 mg of photocatalyst was added. The photocatalytic degradation of rhodamine B solution was performed by using a xenon lamp of 300 W as the visible light source. The rhodamine B solution was stirred with a magnetic stirrer for 60 min in the dark before visible light illumination to ensure that an adsorption–desorption equilibrium was established between the photocatalyst and rhodamine B. Then, the light source was turned on for visible light irradiation, and samples were taken every 30 min, and studied using a spectrophotometer to measure the absorbance of the rhodamine B solution.

Results and discussion

Synthesis and characterization

In this work, three new porphyrin derivatives TCyPPP, TbePPP and TPyPPP were successfully prepared by means of Schiff base connection. The structures of the porphyrin derivatives and their self-assemblies were characterized *via* FT-IR, UV-vis, SEM and ^{1}H NMR. The synthesis routes of 5,10,15,20-tetra(4-aminophenyl)-21h,23h-porphyrin (TAPP), 5,10,15,20-tetra[p-(4-cyanophenylmethylene imino)]phenyl porphyrin (TCyPPP), 5,10,15,20-tetra[p-(P-benzylidene imino)]phenyl porphyrin (TbePPP) and 5,10,15,20-tetra[p-(4-pyridylimethylene imino)]phenyl porphyrin (TPyPPP) are shown in Scheme 1. On the basis of the prepared monomers, three monomers were self-assembled.

The UV-vis absorption spectra of the TAPP, TCyPPP, TbePPP and TPyPPP porphyrin derivatives in dichloromethane solution are shown in Fig. 1(A and B). The three self-assemblies were studied using the UV-vis spectra, as shown in Fig. 1(C). Compared with the monomers, the self-assemblies have better optical properties. After self-assembly of the three monomers, the Soret band showed a significant red shift from about 426 nm to about 460 nm, and a slight split occurred at 434 nm in the Soret band. The Q band for the three monomers appeared in the 500–680 nm visible region, while the Q band for the three self-assemblies appeared at 630–780 nm, and the Q band also showed a significant red shift. In addition, whether it is the Soret band or the Q band, the peak position is obviously widened and the intensity is also significantly stronger. These features indicate that the self-assemblies of TCyPPP, TbePPP and TPyPPP are J-aggregates, which results in a red shift in the absorption spectrum to improve the light absorption in the visible light absorption spectrum. For the Q band, Q has four small absorption peaks in the three monomers, and, after self-assembly, four small absorption peaks disappeared obviously, while a strong absorption peak appeared at 630–780 nm. This may be because the absorption range of the Q band becomes wider and the absorption intensity becomes larger, so the absorption bands overlap, showing only one strong absorption band at the macro level.

FT-IR spectra of the TAPP and TCyPPP, TbePPP and TPyPPP porphyrin derivatives are shown in Fig. 1(D). The characteristic peak of –NH$_2$ was observed at 3348 cm^{-1} in TAPP, which was basically consistent with the known literature. However, there was no corresponding absorption peak in the three porphyrin derivatives of TCyPPP, TbePPP and TPyPPP, indicating that –NH$_2$ disappeared in TCyPPP, TbePPP and TPyPPP. In the infrared spectrum of TCyPPP, TbePPP and TPyPPP, three characteristic stretching vibration peaks were generated at 1613, 1623 and 1603 cm^{-1}, respectively. It indicates that the expected TCyPPP, TbePPP and TPyPPP porphyrin derivatives were successfully coupled with p-cyanobenzaldehyde, benzaldehyde and 4-pyridinyl formaldehyde in the form of a Schiff base through TAPP. In addition, in the infrared spectrum of TCyPPP, the stretching vibration peak of –CN appears at 2229 cm^{-1}. Similarly, in the infrared spectrum of TbePPP, 3021 cm^{-1} is the C–H absorption peak located on the aromatic ring, and there are three weak absorption peaks nearby, and 1573 cm^{-1} is the stretching vibration peak of the aromatic ring C=C skeleton. In the infrared spectrum of TPyPPP, the C–H absorption peak on the pyridine ring is at 3029 cm^{-1} and the vibration peak of the C=C skeleton is at 1552 cm^{-1}. The appearance of these characteristic absorption peaks fully indicates that the expected aldehyde groups in the three aldehydes are successfully linked to the amino group on TAPP, and the three TCyPPP, TbePPP and TPyPPP porphyrin derivatives are successfully synthesized.

The TAPP and TCyPPP, TbePPP and TPyPPP porphyrin derivatives were studied using the ^{1}H NMR spectra using CDCl$_3$ as a solvent. Since the porphyrin compound is a conjugated system having 18 π electrons, it can generate an opposite

induced magnetic field under the action of an external magnetic field. Therefore, the N atom with a high electron cloud density on the porphyrin ring is in strong shielding, and finally the N–H proton signal peak appears at about −2.70 ppm. For TAPP, the proton signal peak of β-H on the porphine ring appears at 8.88 ppm, which belongs to the characteristic peak of typical porphyrin compounds. For the three porphyrin derivatives, as the conjugation range becomes larger, the overall electron cloud density is relatively small, so the shielding effect is reduced, the descreening effect is increased, and the chemical shift of β-H is larger, which appears at 10.06, 10.03 and 10.05 ppm, respectively.

For TAPP, a sharp single peak appeared at 5.30 ppm, attributed to the chemical shift of the H in the amino group, while no corresponding chemical displacement peak was observed in the three porphyrin derivatives TCyPPP, TbePPP and TPyPPP. In contrast, for the three TCyPPP, TbePPP and TPyPPP porphyrin derivatives, a singlet peak appeared at 8.94, 8.95, and 8.81 ppm. This corresponds to the chemical shift of the azo protons (–CH═N–) in the three conjugates, indicating that the three porphyrin derivatives were successfully synthesized. In addition, the ^{1}H NMR spectrum of the coupled TCyPPP has multiple peaks at 7.08–7.62 ppm, which is attributed to the chemical shift of protons on the benzene ring connected to the cyanide group. Similarly, the protons on the benzene ring of coupled TbePPP and the pyridine protons of TPyPPP show multiple peaks in the range of 7.56–8.07 ppm and 7.05–7.61 ppm. The ^{1}H NMR of TAPP and TCyPPP, TbePPP and TPyPPP showed a weak singlet peak around −2.70 ppm, which is attributed to the proton characteristic peak in the porphyrin ring. All these proved that the three porphyrin derivatives were synthesized successfully.

In order to more objectively observe the morphology of the three self-assemblies after self-assembly, the three types of monomers and their self-assemblies were studied by scanning electron microscopy (SEM), as shown in Fig. 2(A–C). In Fig. 2 are scanning electron microscope images of the three monomers, TCyPPP, TbePPP, and TPyPPP, respectively. From the electron microscope image, it can be seen that all three monomers have irregular shapes and appear in a disordered state. In Fig. 2(D–F) are respectively the scanning electron microscope images of the three self-assembled bodies TCyPPP, TbePPP and TPyPPP. It can be clearly seen from the electron microscopy that, after the process of self-assembly, the three kinds of self-assembly have formed a good shape. The self-assembly of TCyPPP has a regular petal-shaped structure. The self-assembly of TbePPP has a spherical morphology, and the self-assembly of TPyPPP has a layered structure with layers of accumulation. All three self-assemblies have a good regular morphology compared to the monomer, indicating the successful preparation of the self-assemblies.

Photocatalytic performance

The photocatalytic properties of the TAPP and TCyPPP, TbePPP and TPyPPP porphyrin derivatives under visible light were studied with the organic pollutant rhodamine B as a representative.
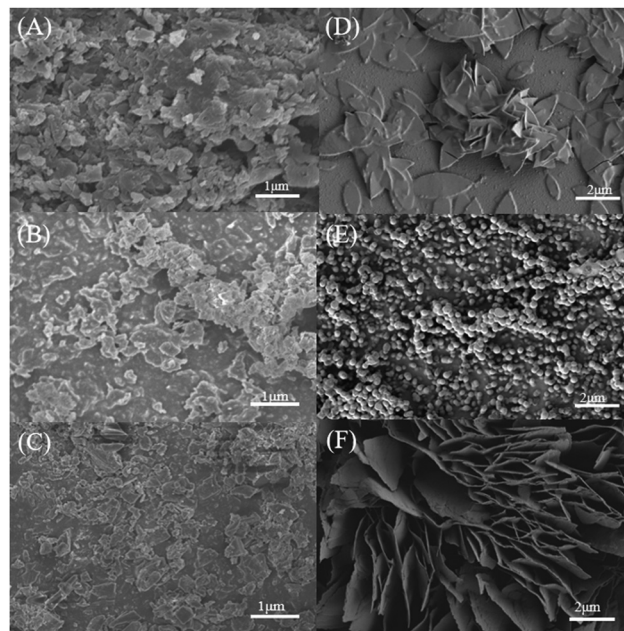

Fig. 2 SEM images of the monomers of (A) TCyPPP, (B) TbePPP and (C) TPyPPP; and self-assemblies of (D) TCyPPP, (E) TbePPP and (F) TPyPPP.

The degradation degree D_t of RhB is calculated by the following formula (1):

$$D_t = \frac{A_0 - A_t}{A_0} \times 100\%. \tag{1}$$

Here, A_0 is the initial absorbance of rhodamine B at the 554 nm absorption and A_t is the absorbance at time t. According to the results of four kinds of photocatalytic degradation, the absorbance measured for RhB at different illumination times was plotted as shown in Fig. 3.

The change curve of the degradation rate of the RhB dye with time by TAPP and the three porphyrin derivatives is shown in Fig. 5(A). In the absence of a photocatalyst, RhB self-degraded by about 10.9% in 3.5 h, as shown in curve 5 in Fig. 5(A), which can be ignored. It is believed that RhB cannot degrade itself under visible light, or it takes a long time to degrade itself. However, the degradation rate of RhB was accelerated after a photocatalyst was added and the degradation amount was greatly increased. After 3.5 h or even less, the degradation rate of RhB reached more than 85%, which is basically considered to achieve complete degradation. Therefore, for the degradation of RhB, it is necessary to help the photocatalyst to achieve the purpose of degradation under visible light.

After the addition of the TAPP catalyst, the degradation rate of RhB reached 88.3% after 3.5 h, and substantially complete degradation was achieved, as shown by curve 1 in Fig. 5(A). Under the same experimental conditions, the degradation rate and degradation time of RhB were significantly accelerated after the addition of the three porphyrin derivative photocatalysts, and the degradation rate reached over 85% within 2.5 h. For catalyst TCyPPP, as shown in curve 2 of Fig. 5(A),
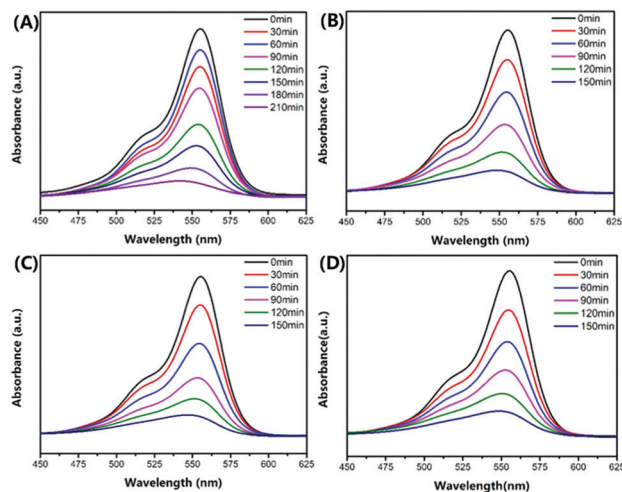
Fig. 3 UV-vis of RhB solution at different illumination times with (A) TAPP, (B) TCyPPP, (C) TbePPP and (D) TPyPPP (the initial concentration of RhB is 1×10^{-5} mol L^{-1}).

the degradation rate reached 86.4% at 2.5 h. For catalyst TbePPP, as shown in curve 3 of Fig. 5(A), the degradation rate reached 88.3%. The degradation rate of catalyst TPyPPP also reached 85.8%, as shown in curve 4 of Fig. 5(A). After TAPP is coupled with three aldehydes *via* a Schiff base, the photocatalytic efficiency can be greatly improved, indicating that the three porphyrin derivatives of TCyPPP, TbePPP and TPyPPP have higher photocatalytic efficiency.

The photocatalytic experiments of RhB were carried out on the three self-assemblies. According to the results of the three porphyrin self-assemblies of photocatalytic degradation, the absorbance measured for rhodamine B under different illumination times was plotted as shown in Fig. 4. The curve of the absorbance measured for RhB under different illumination time conditions as a function of time is shown in Fig. 5(B). It can be seen from the ultraviolet absorption curve of RhB that
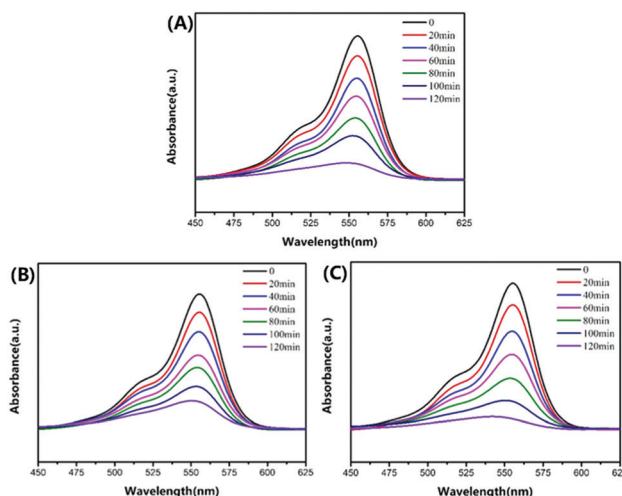

Fig. 4 UV-vis absorption spectra of RhB aqueous solution at different illumination time intervals with the self-assembly of (A) TCyPPP, (B) TbePPP and (C) TPyPPP (the initial concentration of RhB is 1×10^{-5} mol L^{-1}).
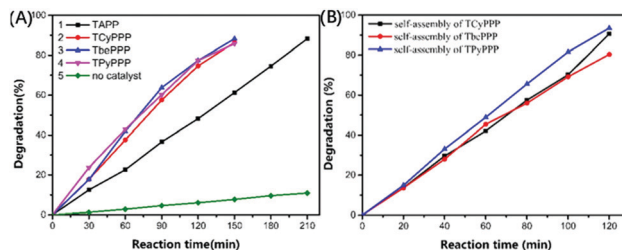

Fig. 5 (A) Degradation efficiency of RhB for TAPP, TCyPPP, TbePPP and TPyPPP. (B) Degradation efficiency of RhB for the self-assembly of TCyPPP, TbePPP and TPyPPP.
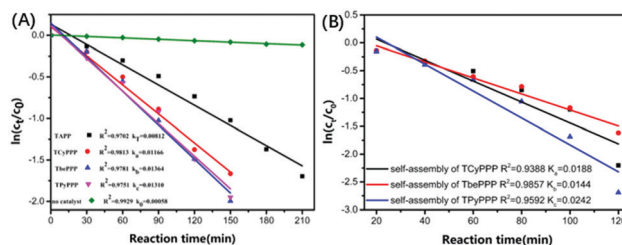

Fig. 6 (A) First order kinetic fitting curve of RhB degradation by TCyPPP, TbePPP and TPyPPP. (B) First order kinetic fitting curve of RhB degradation by the self-assemblies of TCyPPP, TbePPP and TPyPPP.

the three self-assemblies have a good degradation effect on RhB, and substantially complete degradation is achieved in about two hours.

First-order kinetics was used to evaluate the degradation of the RhB dye, and its first-order kinetics equation was expressed by formula (2):

$$\ln\left(\frac{c_t}{c_0}\right) = -k_a t. \tag{2}$$

Here, k_a is the rate constant (min^{-1}). The change curve of $\ln(C_t/C_0)$ with time t (C_0 is the initial concentration of the solution, and c_t is the concentration of the solution at time t) was plotted to study the photocatalytic reaction kinetics, as shown in Fig. 6(A). The rate constants of TAPP and TCyPPP, TbePPP and TPyPPP for RhB under visible light irradiation were 8.12×10^{-3} min^{-1}, 11.66×10^{-3} min^{-1}, 13.64×10^{-3} min^{-1} and 13.10×10^{-3} min^{-1}, respectively. It can be seen from the rate constant that the degradation rate of the three new porphyrin derivatives, TCyPPP, TbePPP and TPyPPP, is significantly higher than that of TAPP, indicating that the catalytic performance of the three new porphyrin derivatives is much higher than that of TAPP. As for the self-degradation of rhodamine B, its degradation rate constant is only 0.58×10^{-3} min^{-1}, which is much lower than the catalytic rate constant of the three catalysts, so the self-degradation of RhB can be ignored. Similarly, Fig. 6(B) shows the first order kinetic fitting curve of self-assembled TCyPPP, TbePPP and TPyPPP degradation of RhB. The rate constants were 18.8×10^{-3} min^{-1}, 14.4×10^{-3} min^{-1} and 24.2×10^{-3} min^{-1}, respectively. The photocatalytic degradation rate constants were also greater than those of the monomers
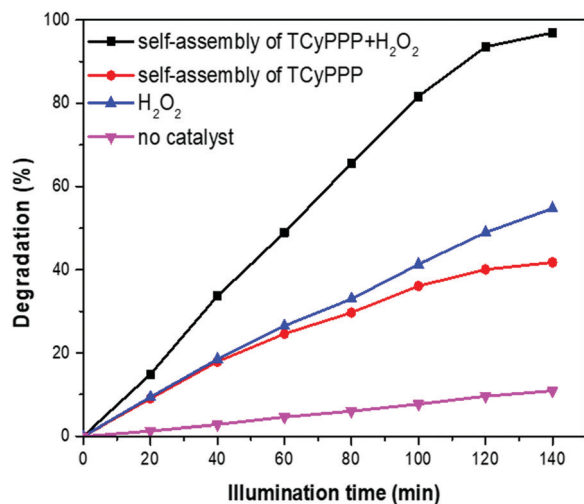
Table 1 Comparison of the photocatalytic properties for RhB pollutant degradation of the three porphyrin derivatives and their self-assemblies and other similar studies

Photocatalysts	Dyes	Photocatalytic rate constant (10^{-3} min^{-1})	References
Graphene@TCPP porphyrin	RhB	6.5	34
Graphene@TiO$_2$@porphyrin	RhB	9.4	36
Porphyrin dicarboxylic acid–TiO$_2$ (PORBP–TiO$_2$)	MB	5.22	37
P-25 Degussa TiO$_2$	RhB	1.2	30 and 36
TCyPPP	RhB	11.66	This study
TbePPP	RhB	13.64	This study
TPyPPP	RhB	13.10	This study
Self-assembly of TCyPPP	RhB	18.8	This study
Self-assembly of TbePPP	RhB	14.4	This study
Self-assembly of TPyPPP	RhB	24.2	This study

under the same conditions. In addition, these rate constants are significantly higher than the photocatalytic performance of porphyrin derivatives reported previously,[34–37] as well as the p-25 Degussa TiO$_2$ photocatalyst (the relative rate constant is only 1.2×10^{-3} min^{-1}), as shown in Table 1.[30,36]

Compared with the three monomers, the self-assemblies have higher catalytic efficiency. The catalytic degradation of RhB in the three self-assemblies reached more than 90% within 2 h, while the degradation rate of RhB was only about 85% after 2.5 h of the three monomers, indicating that the catalytic time of the self-assemblies for RhB is shorter and the catalytic efficiency is higher.
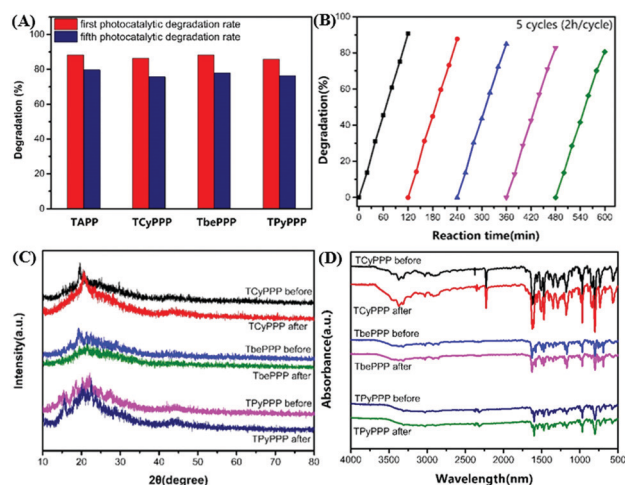
In order to further explore the photocatalytic activity of the three self-assembled compounds, we took TCyPPP as an example to test the photocatalytic efficiency of a blank (only RhB), TCyPPP, H$_2$O$_2$ and TCyPPP + H$_2$O$_2$ (Fig. 7). As can be seen from the figure, the degradation rates of RhB by TCyPPP and H$_2$O$_2$ reached 41.8% and 54.7%, respectively. When TCyPPP and H$_2$O$_2$ acted together to catalyze degradation, the degradation rate reached 96.9% within 140 min, indicating that the two cooperated in the catalytic engineering and significantly improved the photocatalytic degradation effect.

Studies have shown that after the J-aggregation of organics with a π-conjugated structure, electrons in the aggregate can fill the entire aggregate across a single molecule, resulting in a strong π–π interaction, making it a semiconductor material. Therefore, the self-assembled porphyrin can be used as a photocatalyst to collect light energy by using visible light irradiation and generate electron–hole pairs. These electron–hole pairs play an oxidation–reduction role in the degradation of rhodamine B. It also has better photocatalytic efficiency due to its higher charge separation ability.

Reproducibility of the photocatalytic activity

The photostability and repeatability of the photocatalyst are important factors that affect the practical application of the photocatalyst. Therefore, the photostability of the TAPP and TCyPPP, TbePPP and TPyPPP porphyrin derivatives was tested. The photocatalytic degradation rate changes of the TAPP and TCyPPP, TbePPP and TPyPPP porphyrin derivatives after five repeated experiments are shown in Fig. 8(A). Whether it is TAPP or the TCyPPP, TbePPP and TPyPPP porphyrin derivatives, the

Fig. 7 The RhB degradation rates of various catalytic conditions under visible light irradiation in water at room temperature.

Fig. 8 (A) Difference in the photocatalytic degradation rate of TAPP and TCyPPP, TbePPP and TPyPPP before and after the cycling test. (B) Stability test of the photocatalytic activity of the TCyPPP self-assembly. (C) The XRD and (D) the FT-IR tests of the monomers TCyPPP, TbePPP and TPyPPP before and after the photocatalytic cycle experiment.

photocatalytic activity decreased by about 10% after 5 cycles of experiments, indicating that the photocatalytic activity gradually decreased with the cycle period. Taking self-assembled TCyPPP as an example, a photocatalytic cycle experimental test was carried out, and the results are shown in Fig. 8(B). After five cycles of experiments, the photocatalytic degradation rate of self-assembled TCyPPP decreased from 93.5% to 83.2%. Basically, it can be considered that self-assembled TCyPPP also has good photocatalytic stability.

In addition, the monomers TCyPPP, TbePPP and TPyPPP were respectively tested by XRD and FT-IR before and after the photocatalytic cycle experiment. The results are shown in Fig. 8(C and D). The results showed that the monomers TCyPPP, TbePPP and TPyPPP maintained good original framework connectivity during photodegradation, thus demonstrating the good cyclability and high stability of the monomers during photocatalytic degradation.

In addition, we took self-assembled TCyPPP nanoparticles as an example to capture active species during rhodamine B photocatalytic degradation.[38–44] Through a literature review, it was found that ethylenediaminetetraacetic acid disodium salt (EDTA-2Na), isopropanol (IPA) and benzoquinone (BQ) were utilized as the scavengers of h^+, $\bullet OH$ and $\bullet O^{2-}$, respectively.[45–47] Fig. 9 shows the RhB degradation process under different conditions (without H_2O_2). The experimental results showed that the addition of the EDTA-2NA, IPA and BQ scavengers seriously affected the degradation of RhB. This indicates that h^+, $\bullet OH$ and $\bullet O^{2-}$ produced in the photocatalytic process are important active species and play a very important role in RhB degradation.

By referring to the references and the above experimental results, we proposed a possible photocatalytic degradation reaction mechanism, as shown in Fig. 10.[48–51] Firstly, the electronic structure of the porphyrin derivatives was adjusted by coupling TAPP with three aldehydes. The band gap of the three porphyrin derivatives was narrower than that of TAPP,
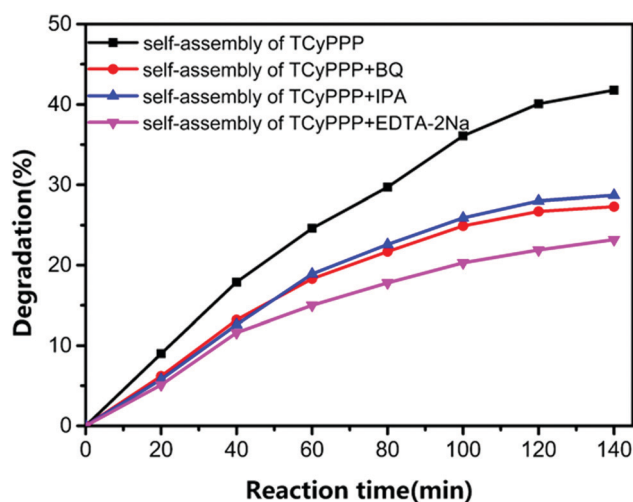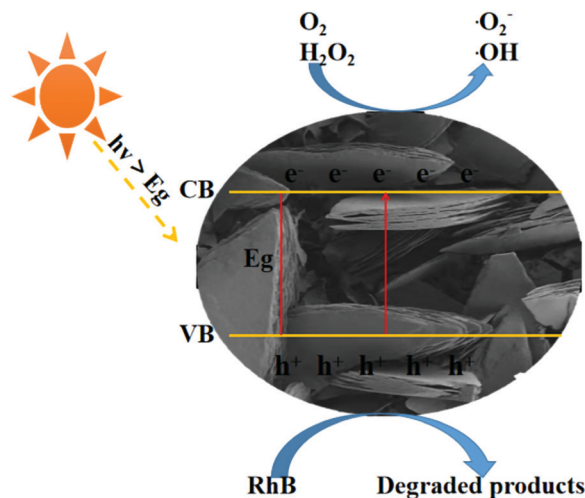

Fig. 10 Reasonable photocatalytic mechanism for RhB under visible light irradiation.

and the valence band (VB) of the photocatalyst is more likely to excite light generation. The electrons are directed to their conduction band (CB). Secondly, electrons in the VB are mainly distributed in the orbital of the photocatalyst before visible light exposure. Under visible light irradiation, visible light absorbed by the photocatalyst transfers energy to H_2O_2 to form h^+. O_2 can get excited electrons and form $\bullet O_2^-$. At the same time, the same number of photogenerated holes (h^+) as photogenerated electrons is left in the VB. h^+, $\bullet OH$ and $\bullet O_2^-$ can effectively degrade rhodamine B molecules, thereby achieving the purpose of catalytic degradation. Finally, since the three porphyrin derivatives have a larger conjugation range, the charge transport speed will be faster, thereby promoting the separation of photogenerated carriers and effectively improving the photocatalytic activity of the catalyst.

Conclusions

Three new porphyrin derivatives, TCyPP, TbePPP and TPyPPP, were synthesized successfully and the three derivatives were self-assembled by the principle of self-assembly. Photocatalytic degradation experiments of rhodamine B were carried out and the photocatalytic activities of the three derivatives and their self-assembled components were evaluated. The photocatalytic experiments show that the catalytic efficiency of the self-assemblies is higher than that of the three monomers and TAPP because of their higher charge separation ability. In addition, the three kinds of self-assembly have good reusability.

Fig. 9 Photogenerated carrier trapping in the system of photodegradation of phenol by self-assembly of TCyPP under visible light irradiation.

Author contributions

Conceptualization: B. Gao and Y. Li. Investigation: J. Pei. Content analysis: J. Pei. Experiments and writing – original draft: J. Pei. Writing – review & editing: B. Gao. All others contributed Project administration: Y. Li and Q. Duan.

Conflicts of interest

There are no conflicts to declare.

Acknowledgements

References

1 C. Lin, W. Zhu, H. Yang, Q. An, C. A. Tao, W. Li, J. Cui, Z. Li and G. Li, *Angew. Chem., Int. Ed.*, 2011, **50**, 4947–4951.

2 M. Mousavi, S. Hosseinnezhad, A. M. Hung and E. H. Fini, *Fuel*, 2019, **236**, 468–479.

3 K. Qian, T. R. Fredriksen, A. S. Mennito, Y. Zhang, M. R. Harper, S. Merchant, J. D. Kushnerick, B. M. Rytting and P. K. Kilpatrick, *Fuel*, 2019, **239**, 1258–1264.

4 Y. Jia, J. Li, J. Chen, P. Hu, L. Jiang, X. Chen, M. Huang, Z. Chen and P. Xu, *ACS Appl. Mater. Interfaces*, 2018, **10**, 15369–15380.

5 B. Purushothaman, J. Choi, S. Park, J. Lee, A. A. S. Samson, S. Hong and J. M. Song, *J. Mater. Chem. B*, 2019, **7**, 65–79.

6 Y. Liu, L. Wang, H. Feng, X. Ren, J. Ji, F. Bai and H. Fan, *Nano Lett.*, 2019, **19**, 2614–2619.

7 P. M. Beaujuge and J. M. J. Frechet, *J. Am. Chem. Soc.*, 2011, **133**, 20009–20029.

8 Z. Zhang, Y. Zhu, X. Chen, H. Zhang and J. Wang, *Adv. Mater.*, 2019, **31**, e1806626.

9 X. F. He, M. Chen, R. Chen, X. Zhu, Q. Liao, D. D. Ye, B. Zhang, W. Zhang and Y. X. Yu, *J. Hazard. Mater.*, 2018, **358**, 346–354.

10 J. Y. Li, J. H. Li, Q. P. Chen, J. Bai and B. X. Zhou, *J. Hazard. Mater.*, 2013, **262**, 304–310.

11 Y. Z. Chen, A. X. Li, X. Q. Yue, L. N. Wang, Z. H. Huang, F. Y. Kang and A. A. Volinsky, *Nanoscale*, 2016, **8**, 13228–13235.

12 M. O. Senge, S. A. MacGowan and J. M. O'Brien, *Chem. Commun.*, 2015, **51**, 17031–17063.

13 G. B. Bodedla, J. Huang, W. Wong and X. Zhu, *ACS Appl. Nano Mater.*, 2020, **3**, 7040–7046.

14 A. D. Schwab, D. E. Smith, B. Bond-Watts, D. E. Johnston, J. Hone, A. T. Johnson, J. C. De Paula and W. F. Smith, *Nano Lett.*, 2004, **4**, 1261–1265.

15 S. Mandal, S. Bhattacharyya, V. Borovkov and A. Patra, *J. Phys. Chem. C*, 2011, **115**, 24029–24036.

16 S. Mandal, S. Bhattacharyya, V. Borovkov and A. Patra, *J. Phys. Chem. C*, 2012, **116**, 11401–11407.

17 T. Arai, M. Tanaka and H. Kawakami, *ACS Appl. Mater. Interfaces*, 2012, **4**, 5453–5457.

18 N. Zhang, L. Wang, H. Wang, R. Cao, J. Wang, F. Bai and H. Fan, *Nano Lett.*, 2018, **18**, 560–566.

19 Y. Zhong, J. Wang, R. Zhang, W. Wei, H. Wang, X. Lü, F. Bai, H. Wu, R. Haddad and H. Fan, *Nano Lett.*, 2014, **14**, 7175–7179.

20 J. Wang, Y. Zhong, L. Wang, N. Zhang, R. Cao, K. Bian, L. Alarid, R. E. Haddad, F. Bai and H. Fan, *Nano Lett.*, 2016, **16**, 6523–6528.

21 J. Wang, Y. Zhong, L. Wang, N. Zhang, R. Cao, K. Bian, L. Alarid, R. E. Haddad, F. Bai and H. Fan, *Nano Lett.*, 2016, **16**, 6523–6528.

22 A. F. Molina-Osorio, D. Cheung, C. O'Dwyer, A. A. Stewart, M. Dossot, G. Herzog and M. D. Scanlon, *J. Phys. Chem. C*, 2020, **124**, 6929–6937.

23 J. Hou, P. Lei, T. Meng, F. Zhao, H. Xu, X. Li, K. Deng and Q. Zeng, *Langmuir*, 2020, **36**, 9810–9817.

24 J. Li, W. Sun, Z. Yang, G. Gao, H. Ran, K. Xu, D. Duan, X. Liu and F. Wu, *ACS Appl. Mater. Interfaces*, 2020, **12**, 54378–54386.

25 T. Kim, S. Ham, S. H. Lee, Y. Hong and D. Kim, *Nanoscale*, 2018, **10**, 16438–16446.

26 M. D. Aljabri, D. D. La, R. W. Jadhav, L. A. Jones, D. D. Nguyen, S. W. Chang, L. D. Tran and S. V. Bhosale, *Fuel*, 2019, **254**, 115639.

27 M. D. Aljabri, R. W. Jadhav, M. Al Kobaisi, L. A. Jones, S. V. Bhosale and S. V. Bhosale, *ACS Omega*, 2019, **4**, 11408–11413.

28 Y. Zhong, Z. X. Wang, R. F. Zhang, F. Bai, H. M. Wu, R. Haddad and H. Y. Fan, *ACS Nano*, 2014, **8**, 827–833.

29 P. Guo, P. Chen and M. Liu, *ACS Appl. Mater. Interfaces*, 2013, **5**, 5336–5345.

30 D. Duc La, A. Rananaware, H. P. Nguyen Thi, L. Jones and S. V. Bhosale, *Adv. Nat. Sci.: Nanosci. Nanotechnol.*, 2017, **8**, 015009.

31 D. D. La, H. P. N. Thi, Y. S. Kim, A. Rananaware and S. V. Bhosale, *Appl. Surf. Sci.*, 2017, **424**, 145–150.

32 D. Wang, L. J. Niu, Z. Y. Qiao, D. B. Cheng, J. F. Wang, Y. Zhong, F. Bai, H. Wang and H. Y. Fan, *ACS Nano*, 2018, **12**, 3796–3803.

33 Y. Zhou, Y. Huang, B. Jin, X. Luo and Z. Liang, *Ind. Eng. Chem. Res.*, 2018, **58**, 44–52.

34 D. La, R. Hangarge, S. V. Bhosale, H. Ninh, L. Jones and S. Bhosale, *Appl. Sci.*, 2017, **7**, 643.

35 D. D. La, S. V. Bhosale, L. A. Jones and S. V. Bhosale, *Photochem. Photobiol. Sci.*, 2017, **16**, 151–154.

36 D. D. La, S. V. Bhosale, L. A. Jones, N. Revaprasadu and S. V. Bhosale, *ChemistrySelect*, 2017, **2**, 3329–3333.

37 J. Ryu, R. S. Kumar and Y. A. Son, *J. Nanosci. Nanotechnol.*, 2020, **20**, 6266–6273.

38 L. Jing, Y. Xu, S. Huang, M. Xie, M. He, H. Xu, H. Li and Q. Zhang, *Appl. Catal., B*, 2016, **199**, 11–22.

39 L. Guo, Q. Zhao, H. Shen, X. Han, K. Zhang, D. Wang, F. Fu and B. Xu, *Catal. Sci. Technol.*, 2019, **9**, 3193–3202.

40 X. Gao, K. Gao, X. Li, Y. Shang and F. Fu, *Catal. Sci. Technol.*, 2020, **10**, 372–381.

41 D. Wang, L. Yue, L. Guo, F. Fu, X. He and H. Shen, *RSC Adv.*, 2015, **5**, 72830–72840.

42 D. Wang, G. Xue, Y. Zhen, F. Fu and D. Li, *J. Mater. Chem.*, 2012, **22**, 4751–4758.

43 D. Wang, H. Shen, L. Guo, F. Fu and Y. Liang, *New J. Chem.*, 2016, **40**, 8614–8624.

44 D. Wang, L. Guo, Y. Zhen, L. Yue, G. Xue and F. Fu, *J. Mater. Chem. A*, 2014, **2**, 11716–11727.

45 C. Liu, X. Cui, Y. Li and Q. Duan, *Chem. Eng. J.*, 2020, **399**, 125807.

46 R. Cheng, G. Li, L. Fan, J. Jiang and Y. Zhao, *Chem. Commun.*, 2020, **56**, 12246–12249.

47 X. Cui, Y. Li, W. Dong, D. Liu and Q. Duan, *React. Funct. Polym.*, 2020, **154**, 104633.

48 B. C. Ma, S. Ghasimi, K. Landfester, F. Vilela and K. A. I. Zhang, *J. Mater. Chem. A*, 2015, **3**, 16064–16071.

49 H. Q. Li, Y. X. Liu, X. Gao, C. Fu and X. C. Wang, *ChemSusChem*, 2015, **8**, 1189–1196.

50 Y. S. Li, M. X. Liu and L. Chen, *J. Mater. Chem. A*, 2017, **5**, 13757–13762.

51 A. Li, H. X. Sun, D. Z. Tan, W. J. Fan, S. H. Wen, X. J. Qing, G. X. Li, S. Y. Li and W. Q. Deng, *Energy Environ. Sci.*, 2011, **4**, 2062–2065.